Int. J. Electron. Commun. (AEÜ) 202 (2025) 156036

Contents lists available at ScienceDirect

Int. J. Electron. Commun. (AEÜ)

journal homepage: www.elsevier.com/locate/aeue

Regular paper

Study of the insertion of corrugations in microwave filters for mitigation of the multipactor effect

S.M. Bonte [a], R. García [a], A. Coves [a,*], J.M. García-Barceló [b], A.A. San-Blas [a], M. Sancho [a], M.A. Sánchez-Soriano [c], V.E. Boria [d]

[a] Department of Communications Engineering-I3E, Miguel Hernandez University of Elche, Elche, Spain
[b] Max Planck Institute for Physics (Werner-Heisenberg-Institut), Munich, Germany
[c] Department of Physics, Systems Engineering and Signal Theory, University of Alicante, Alicante, Spain
[d] Department of Communications-iTEAM, Technical University of Valencia, Valencia, Spain

ARTICLE INFO

Keywords:
Filter
Microwave
Multipactor

ABSTRACT

The multipactor effect is an electron avalanche type discharge, that poses a significant challenge in radiofrequency and microwave high-power devices operating under high-vacuum conditions, affecting their signal integrity and device performance. In this paper, we propose to apply a corrugated surface profile over the inner metallic walls in several microwave components, especially filters, to mitigate this undesired effect. Through numerical simulations, we demonstrate that the introduction of a corrugated surface over critical areas of the component significantly increases the multipactor power threshold. The corrugated profile effectively disrupts the conditions leading to the electron avalanche formation, thereby increasing the breakdown threshold level. We explore the influence of both the geometric parameters of the corrugated profile, and the critical region where it should be placed in the microwave component, providing insights into the optimal design considerations to alleviate this phenomenon. Our findings not only contribute to a broader understanding of the multipactor mitigation techniques in radiofrequency and microwave high-power components, but also offer valuable guidance for their application with a band-pass filter example, resulting in a substantial improvement of its multipactor power threshold after introducing the corrugated surface profile, while maintaining the electric performance of the originally designed component. Moreover, the proposed solution outstands other state-of-the-art multipactor reduction techniques, by avoiding the use of material coatings, micro-porous surfaces as well as non-standard waveguides, thus confirming very good prospects for its use with filtering components in high power demanding applications, such as satellite communication systems.

1. Introduction

One of the main challenges that microwave space components designers usually face, is the improvement of their ability to withstand the increasingly higher radiofrequency (RF) power requirements that must be considered at the output of transmitter stages. Nevertheless, and despite such efforts, these designs usually suffer from the multipactor effect [1]. Multipactor can be present in a wide variety of scenarios, such as satellite communication payloads and particle accelerators, for instance. This undesired effect occurs due to the generation of an avalanche of electrons in the component under vacuum conditions, dealing with high power and high frequency signals. It strongly depends on the surface material property known as the Secondary electron Emission Yield (SEY). This avalanche produces a resonant discharge inside the component with many possible harmful consequences. Among them, we can mention noise increase and consequent signal degradation, local thermal heating, damage on the surface area where it occurs, and even the physical damage of the component, all of which finally lead to a limitation of the real power level for satellite operations. Thus, in the last decades, microwave space component designers have focused their attention on the study of the multipactor effect in the scenario of RF satellite payloads. This has been done in several types of microwave waveguides with different geometries, including empty waveguides [2–7], and also partially dielectric-loaded waveguides [8–11].

Different possible solutions have been addressed to minimize an electron discharge, and the damage it may cause, like using material coatings or micro-porous surfaces with low SEY, obtaining an increase in the multipactor power threshold level (P_{TH}) of the component. These surface coatings reduce the multipactor effect, but their lifetime

* Corresponding author.
E-mail address: angela.coves@umh.es (A. Coves).

https://doi.org/10.1016/j.aeue.2025.156036
Received 23 April 2025; Accepted 8 September 2025
Available online 16 September 2025

still need to be demonstrated in order to become a real optimum solution for space applications [12–14]. Furthermore, the effect of an irregular micro-porous surface depends on the details of the manufacturing process, and may yield to unacceptable variations from one piece to another [13]. An alternative possible solution is to design the waveguide component in such a way that its electromagnetic (EM) field distribution may prevent the discharge. This can be done either avoiding regions of high field intensity and/or small gaps [15], or modifying the waveguide cross-section, like in [16], where a wedge-shaped hollow waveguide (instead of a conventional rectangular one) proved to deviate the resonant paths of the electrons toward regions with lower voltages. In both cases, the multipactor power threshold levelr level is typically increased. Also, high-power low-pass harmonic filters in rectangular waveguide technology showed an improved power-handling performance, by simply using a sinusoidal profile along the propagation direction [17]. However, the use of non-standard waveguides makes it necessary the design of expensive and bulky waveguide transformers. More recently, new approaches have been addressed, like applying an electrostatic field inside the component for suppressing multipactor breakdown [18], or introducing dielectric material [19, 20] or ridged structures [21] in microwave devices, although they do not meet the highly restrictive requirements, in terms of quality factor or compactness, requested for filtering components used in space applications.

Alternatively, preliminary studies have been performed in which different profiles of 1-D or 2-D metallic corrugations over the double-metal-surface of a waveguide have proven to increase the multipactor P_{TH} [22–24], although it has only been studied in canonical waveguides.

The present study focuses on exploring the impact of different corrugation profiles, including rectangular and triangular shapes, as well as their size, ranging from dimensions of the order of tens of microns up to the millimeter. Not only do we aim to understand how these parameters affect the effectiveness in suppressing the multipactor effect, but also to assess the feasibility of implementing these corrugations in critical areas of a real filtering structure. This approach intends to explore the capability of these techniques on more complex components, and to open up new possibilities for design and optimization of passive devices for microwave space applications.

2. Corrugation profiles effect on rectangular waveguides

In this section, we explore the impact of different profiles of metallic corrugations on the resulting multipactor power threshold on rectangular waveguides. In this regard, the boundary conditions of the fields within the corrugated regions (which make that there is no tangential field over the metal surfaces) make that the field intensity inside the corrugations, which is responsible of driving out the secondary electrons emitted at the inner surfaces of the corrugations, is significantly reduced. When comparing different corrugation profiles, like those with rectangular or triangular shapes, a key difference in terms of multipactor is that, in the triangular configuration case, there is also almost no surface, and consequently, no field between corrugations, because nearly no space needs to be left between them. However, this is not the case in other possible corrugation profiles, which could be manufactured with metallic 3D printing or Computer Numerical Control (CNC) techniques, like in the rectangular case, in which certain horizontal surfaces must be kept between corrugations, where the field intensity (above the horizontal metal surfaces) does not vanish. Although alternative corrugated profiles (avoiding horizontal surfaces) could be more optimal for this problem (such as 3-D metallic profiles, with conical or pyramidal shapes, that mimic the geometry of the absorbing material in anechoic chambers), we believe that increased complexity may arise in their fabrication process, along with higher insertion losses. Thus, we have first considered a rectangular profile, and secondly, a triangular one, for comparison purposes.

In this work, such two profiles have been applied to both, the top and bottom surfaces of a rectangular waveguide (RW). Differently from classical solutions based on the use of material coatings with low SEY, in the proposed approach, the significant reduction of the multipactor effect achieved is caused by the decrease of the EM field intensity near the periodic grooves. Consequently, the electron staid time and the temporal dispersion of the secondary electron generation are increased. In this way, the generated secondary electrons are deviated from the resonant phase associated with the double-surface resonant multipactor effect.

The results of the comparative study of the P_{TH} level at which multipactor occurs are shown next. For this purpose, the effect is first analyzed on a non-standard aluminium RW (a finite conductivity value of $3.8 \cdot 10^7$ S/m has been considered) of width $a = 22.86$ mm, height $b = 0.4$ mm (a reduced height to obtain measurable threshold power values) and length $l = 18$ mm with smooth metallic surfaces, considered as a reference, and whose insertion loss is lower than 0.1 dB in the waveguide operating band. A lower conductivity value will translate into a lower level of available field in the component for the same input power and, therefore, it will have a direct relationship with the value of the P_{TH}, which will be increased.

The magnitude of the electric field distribution in the central part of the cross section of this waveguide is shown in Fig. 1(a) (for a power level of 1 W at the waveguide input port), with a maximum value close to 14 kV/m. The EM fields of all analyzed waveguides and filters have been obtained with the full-wave EM analysis tools HFSS [25] and CST Studio Suite [26], whose simulation methodology and boundary conditions are detailed in [27], while the software tool used to study the multipactor effect on the RWs is SPARK3D -as part of CST Studio Suite- [26]. The tool SPARK3D first imports the EM fields inside the component (previously computed with HFSS in this case), and then tracks the resulting electron motion by solving the 3-D Lorentz force equation. In order to perform all the accurate multipactor simulations included in this article with SPARK3D, a homogeneous electron seeding of 10^4 initial electrons has been defined inside the component under study, and the SEY of aluminium material ($\delta_{max} = 2.92$, $\delta_0 = 0.8$, $E_1 = 17$ eV, $E_{max} = 276$ eV) has been used. This practical information has been extracted from the corresponding European Cooperation for Standardization (ECSS) document [28]. The computed P_{TH} value of this waveguide without corrugations, at a frequency of 10.7 GHz (corresponding to a possible experimental test campaign to be performed in this waveguide in the near future, which is within its monomode frequency range), is found to be 1.07 kW.

2.1. Corrugations with a rectangular surface profile with different periodicities

The first proposed corrugated surface profile is a rectangular profile in which rectangular grooves are made longitudinally over the horizontal walls of the waveguide along the propagation direction, characterized by the depth t and width s of the grooves (see Fig. 2), and keeping the same equivalent waveguide height $b_{eq} = 0.4$ mm. The depth of the grooves has been fixed to $t = 50$ μm, which has been chosen small compared to the waveguide height, so that the field distribution in the corrugated waveguide is hardly modified with respect to the reference waveguide with smooth surfaces, for a fair comparison, being the insertion loss in the waveguide operating band lower than 0.1 dB in all cases. Thus, with this rectangular surface profile, here we study the effect of the periodicity $p = s + t$ of the corrugations in the P_{TH} obtained, being s the width and t the depth of the grooves. In particular, we have analyzed two different periodicities. Firstly, with $t = s = 50$ μm (see Fig. 2(a)) and secondly, with the same depth t but width of $s = 75$ μm, as can be seen in Fig. 2(b). This type of corrugated profile can be manufactured using laser milling techniques. In both cases, we have checked that the S-parameters of the corrugated waveguide with respect to the reference waveguide ports are not significantly disturbed

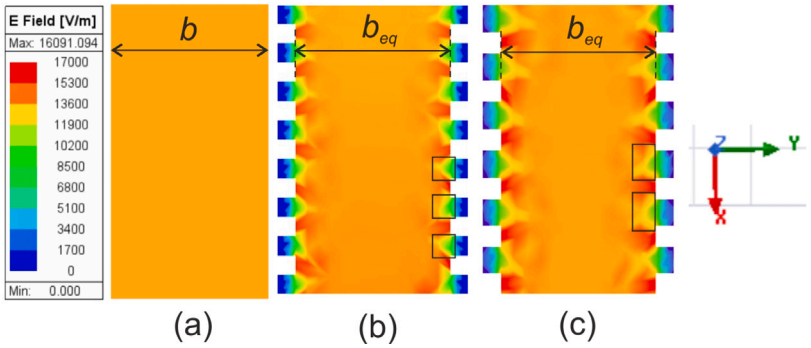

Fig. 1. Electric field intensity in the central part of the waveguide cross section under study with (a) smooth surfaces, and with a rectangular surface profile on the horizontal surfaces with (b) $t = s = 50$ μm, and (c) $t = 50$ μm and $s = 75$ μm. The black squares show some regions between the grooves where there is still a high field intensity.

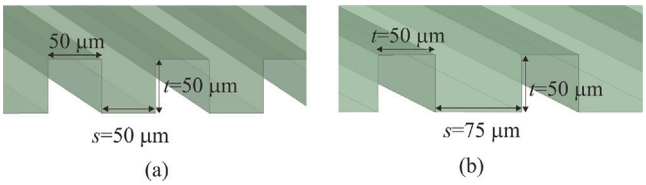

Fig. 2. Rectangular profile with (a) $t = s = 50$ μm, and (b) $t = 50$ μm and $s = 75$ μm.

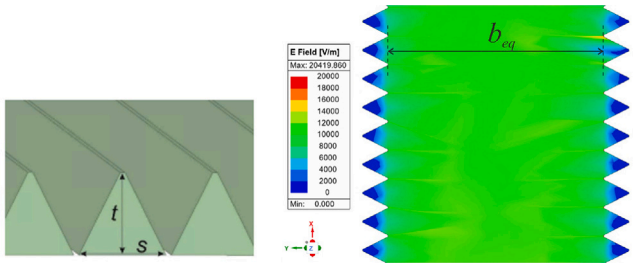

Fig. 3. (a) Triangular surface profile defined by the width s and depth t of the 3D triangular corrugations. (b) Electric field intensity in the waveguide with corrugations of $s = t = 50$ μm.

by the corrugations, i.e. $|S_{11}| < -25$ dB in the corrugated waveguide operating band. On the other hand, we have also checked that the insertion loss in the corrugated waveguide is hardly modified with respect to the case without corrugations, which will be a key point when introducing corrugations in microwave filters, as will be shown later.

Fig. 1(b) and (c) show the magnitude of the electric field distribution in the cross section (central region) of the corrugated waveguide (again for a power level of 1 W at the waveguide input port), and as can be seen, it remains approximately constant with the y-coordinate, with a value close to 14 kV/m, except in the proximity of the corrugations, where the field is highly reduced over the grooves (see black squares in Fig. 1(b) and (c)), although in the region between the grooves there is a high field intensity. In the case with a periodicity of 125 μm (see Fig. 1(c) where $s = 75$ μm), the region with reduced field intensity (over the grooves) is a bit more extense. Considering that the multipactor effect is strongly influenced by the electric field intensity in the areas where secondary electrons are emitted, an increase of the P_{TH} is expected in both cases compared with the waveguide with smooth surfaces. Moreover, since the area with reduced field intensity in the regions over the grooves in the case with a periodicity of 125 μm ($s = 75$ μm) is bigger, a higher P_{TH} is expected to be obtained in this case. The computed P_{TH} for the case of $s = 50$ μm is 2.69 kW (which is also included in Table 1), while a slightly higher P_{TH} value of 2.78 kW has been obtained for the case of $s = 75$ μm. Thus, in the case of rectangular corrugations with the same depth, wider grooves give rise to a slight increase in terms of P_{TH}. Comparing the P_{TH} value obtained in both cases with that of the waveguide with smooth surfaces (1.07 kW), an increase of approximately 1.7 kW is achieved, which represents an improvement of 160%. Although the results are promising, the region between the grooves, with high field intensity, is still prone to produce an electron discharge. A possible solution to this problem will be applied next by considering corrugations with a triangular surface profile.

2.2. Corrugations with a triangular surface profile with different sizes

In a previous study [23], the effect of introducing corrugations with a triangular surface profile with different depth and orientation with respect to the propagation direction was analyzed (in the same RW as in the previous Section 2.1). This study revealed that the most effective strategy to increase the P_{TH} was the implementation of triangular profile corrugations placed longitudinally to the propagation direction, which were chosen with a depth and width of $s = t = 50$ μm. The triangular profile of these corrugations is shown in Fig. 3(a), where a small chamfer of 3 μm is introduced at the peaks and valleys for practical implementation. With this profile, a P_{TH} of 3.72 kW was achieved, as can be seen in Table 1, revealing that this triangular surface profile offers the best P_{TH} results among all previous ones. This is due to a higher reduction of the field intensity in the vicinity of the corrugations in such configuration (see Fig. 3(b)), differently from the rectangular surface profile. This is because the proposed triangular profile shows no flat regions with high field intensity where secondary electrons may be accelerated, thus causing an electron discharge.

Table 1
Comparison of the computed P_{TH} in a non-standard aluminium RW ($a = 22.86$ mm, $b = 0.4$ mm) with different corrugation profiles on the horizontal walls.

Type of corrugated surface profile	P_{TH} (kW)
No corrugations	1.07
Rectangular grooves with $t = s = 50$ μm	2.69
Rectangular grooves with $t = 50$ μm and $s = 75$ μm	2.78
Triangular grooves with $t = s = 50$ μm	3.72

Taking this in mind, next we will study the dependence of the size of the corrugations in this triangular surface profile on the resulting P_{TH} in the waveguide where it is applied. For this purpose, a rectangular waveguide with the same width and length as in Section 2.1 ($a = 22.86$ mm and $l = 18$ mm), but with a higher height of $b = 5$ mm has been chosen, so the effect of bigger corrugations can be analyzed without perturbing the transmission characteristics of this waveguide (see Fig. 4). Again, the P_{TH} value of this waveguide without

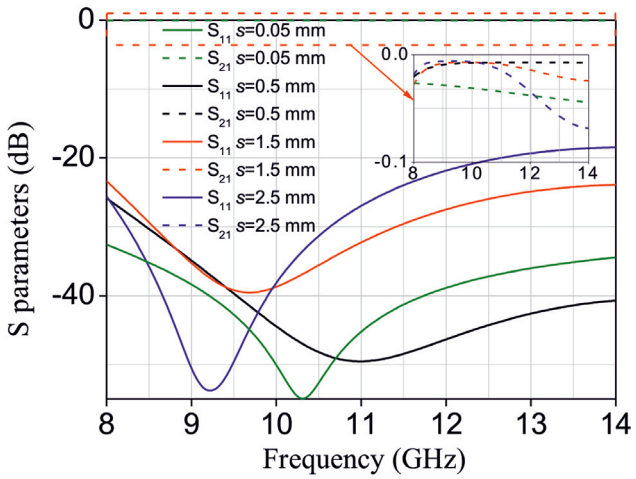

Fig. 4. S-parameters of a section of l = 18 mm of the corrugated rectangular waveguide of dimensions a = 22.86 mm and b = 5 mm with different size of the triangular corrugations, being $s = t$ in all cases (a section of 1 mm of waveguide with smooth walls at the ports ends has been added). (For interpretation of the references to color in this figure legend, the reader is referred to the web version of this article.)

corrugations has been computed, as a reference, obtaining 22.97 kW. Next, P_{TH} has been studied when inserting triangular corrugations of different sizes over the inner horizontal metallic walls of this waveguide, maintaining an equivalent height of b_{eq} = 5 mm, equal to the original height of the rectangular waveguide without corrugations. In all cases, corrugations with a triangular profile placed longitudinally to the direction of propagation have been applied. The S-parameters of this waveguide with different corrugation dimensions have been obtained with respect to the reference waveguide ports (with smooth surfaces), by adding a 1 mm long section of the reference waveguide at its ends, in order to check the range of the corrugation dimensions where the electrical response of the waveguide is hardly modified by the corrugations, as shown in Fig. 4. Corrugations with the following dimensions (in mm) have been studied: $s = t$ = 0.05, 0.5, 1.5 mm and 2.5 mm. This last value is the limit for which the electrical response of the waveguide is not significantly disturbed by the corrugations, i.e. $|S_{11}| < -25$ dB in the waveguide operating band (see also the blue curves related to the s = 2.5 mm case). Additionally, we have checked that the insertion loss in all cases is hardly increased with respect to the waveguide of aluminium without corrugations, being in all cases lower than 0.07 dB in the waveguide operating band. The computed P_{TH} in these cases ranges from 66.87 kW for 0.05 mm corrugations up to 105.46 kW for 0.5 mm corrugations, and from this size of corrugations, the P_{TH} starts to decrease again. Having these results in mind, as a general rule, we can conclude that a greater depth and width of the corrugations provides a higher P_{TH} value, up to a certain limit, which in this waveguide is of about 0.5 mm, from which the P_{TH} is no longer increased. However, a particular study of the dependence of the corrugation dimensions on the obtained P_{TH} should be performed in each particular microwave component.

3. Multipactor analysis of more complex microwave components with corrugations

In this section, we have analyzed the multipactor effect of more complex microwave components that might suffer from the multipactor phenomenon, such as filters at the output stages of satellite communication payloads. It is important to note that filtering structures, differently from waveguides, suffer the effect of field amplification in their resonant cavities, and they can have relatively low P_{TH} levels within their passbands. Afterwards, we will introduce corrugations in such critical areas using a triangular surface profile, which has resulted more effective to mitigate the multipactor effect. Both the resulting electrical response and the new P_{TH} value will be obtained. The configuration used in this section to perform all multipactor simulations is the same as the one described before in Section 2 of this article.

To this end, we have chosen a 3rd-order waveguide band-pass filter with interdigital configuration loaded with metallic strips of flat geometry (Fig. 5(a) displays the analyzed filter with corrugations) made of aluminium and operating at S-band, with a center frequency of 3 GHz and a bandwidth of 200 MHz. This filter was initially designed in [27], and its electrical response is represented in Fig. 6 with black line, obtaining an insertion loss (IL) mean value of 0.1 dB in the nominal passband (2.9–3.1 GHz). To be able to compare P_{TH} results, this parameter is first obtained without the insertion of corrugations. For this purpose, we have first identified the critical zones of the proposed microwave filter where the field intensity is higher, and therefore more prone to suffer a multipactor discharge.

Fig. 5(b) shows the electric field distribution in this filter computed at f_0 = 3 GHz (with values scaled for an input power level of 1 W), which reveals a high concentration of the electric field around all the metallic strips. Therefore, a multipactor analysis in several isolated regions of the filter is required to identify the critical zones in terms of multipactor. We have identified that the critical areas in this structure are the flat surfaces of the first and last resonator strips along with the front and back walls of the rectangular enclosure facing such strips (where the distance is of 3 mm), where the electromagnetic fields are more intense. These zones are the most critical regions in terms of the multipactor phenomenon. We have computed the P_{TH} value at the central frequency of the filter (f_0 = 3 GHz), and also at the frequencies f_1 = 2.86 GHz and f_2 = 3.15 GHz where the S_{21} parameter group delay and stored energy are maximum, and thus more prone to a multipactor discharge. The obtained results are: P_{TH,f_0} = 170 W, P_{TH,f_1} = 72.8 W and P_{TH,f_2} = 83.5 W. Although the obtained multipactor power thresholds are lower at frequencies f_1 and f_2, in practice, the frequency bandwidth of the employed signals do not usually reach such extreme values, so in the following we will focus on the obtained value of P_{TH} at the center frequency of the filter.

Subsequently, we have placed triangular corrugations of 0.5 mm width and depth over the front and back walls of the rectangular enclosure of the filter, above the coaxial ports (see Fig. 5(a)), and whose electric field distribution at 3 GHz (represented in Fig. 7) shows a decrease of the field intensity inside the corrugations, as expected. Once again, this reduction of the electric field intensity, when applying corrugations over the critical surfaces of the component, leads to an increase of the P_{TH}, now obtaining a value of 420 W at the center frequency of the filter, which represents an improvement of 147%. However, although the modified filter with corrugations shows an improved power performance, its electrical response does not meet the original filter specifications in terms of return losses (RL > 25 dB) (see the electrical response of the original filter in Fig. 6 represented in black line), as can be seen in Fig. 6 with green line, showing that RL < 15 dB in the frequency range [3.015–3.07] GHz. Thus, the modified filter with corrugations needs to be redesigned in order to recover the original filter response.

3.1. Optimization of the modified filter by adding an offset Δl to improve the RL within the passband

A first attempt to recover the original filter response in the modified filter with corrugations has been made, through the modification of the distance l between the metal strip closest to the excitation and the plane where the coaxial excitation is located, which was originally fixed to 3 mm for this filter, by adding an offset Δl (see Fig. 5(a)). Fig. 6 shows that, when this offset Δl has a value of −0.3 mm, RL > 25 dB within the passband, and IL < 0.11 dB, revealing that the introduction

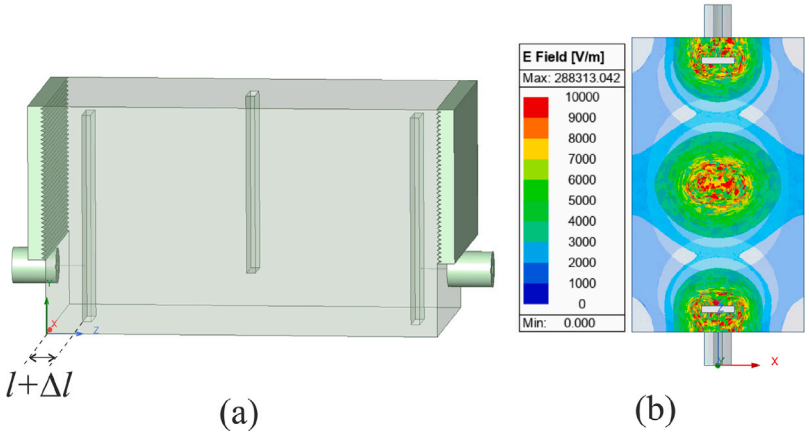

Fig. 5. (a) 3D model of the interdigital 3rd-order band-pass filter with corrugations inserted over the vertical walls above the coaxial ports. (b) Electric field distribution (f_0 = 3 GHz) in the original filter without corrugations.

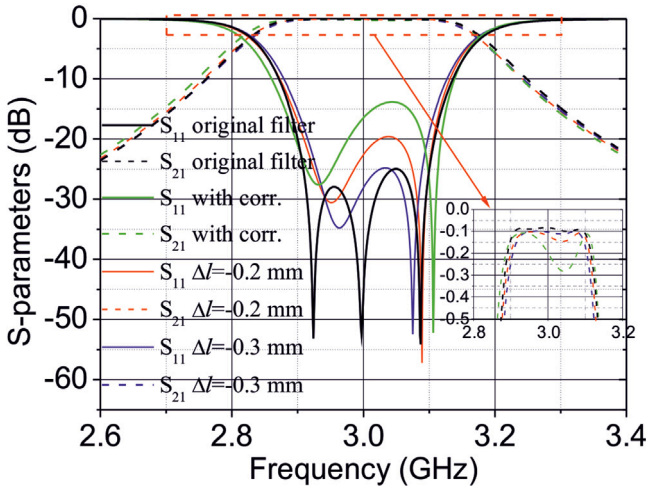

Fig. 6. S-parameters of the filter without and with corrugations, for different values of the Δl-parameter adjusted to improve the RL within the passband. (For interpretation of the references to color in this figure legend, the reader is referred to the web version of this article.)

of corrugations does not increase the insertion losses of the filter (provided that a good matching is achieved in the passband). However, the response does not yet meet the original filter specifications in terms of center frequency and bandwidth, so alternative methods for recovering the original filter response are studied next for this filter.

3.2. Optimization of the modified filter by changing the number of corrugations

A different approximation to recover the frequency response of the original filter (without modifying the aforementioned distance l, i.e., with Δl = 0 mm) consists of reducing the number of corrugations inserted over the vertical walls of the band-pass filter, beginning from the coaxial ports side. We have consecutively removed the nearest corrugations to the coaxial ports in several stages, being removed 5, 8, 12, and finally 15 corrugations, keeping the corrugations in the region where the electric field is maximum, i.e., near the open-ended terminations. For each case, the electrical response is compared to that of the original filter without corrugations. Eventually, the P_{TH} parameter has been also computed for each case to make sure that an increase in the P_{TH} value is still obtained, as this is the original aim of the insertion of the corrugations.

Table 2
Change in P_{TH} when removing different number N of corrugations.

N	P_{TH} (W)
0	420
5	388
8	376
12	345
15	291

In Fig. 8 it can be seen that removing 12 or 15 corrugations results in a frequency response very close to that of the original filter without corrugations. In Table 2 it can be observed that the P_{TH} is progressively reduced as more corrugations are removed, as expected. Thus, although the reduction of some corrugations near the coaxial ports provides an improved electrical response, the P_{TH} value is considerably reduced. As a conclusion, a trade-off between the obtained P_{TH} and the electrical response must be reached, and the case when removing 12 corrugations may be a good compromise, where the electrical response of the filter is very close to that of the original filter without corrugations, while the P_{TH} value has been reduced from 420 to 345 W (a reduction lower than 20%). Therefore, a different optimization approach is explored next to address this limitation.

3.3. Redesign of the modified filter

This new optimization approach consists of redesigning the interdigital filter with corrugations, with the aim of recovering an electrical response similar to the one obtained with the original filter without corrugations. The 3D model of the original filter with its main dimensions is shown in Fig. 9, and its electrical response was represented in Fig. 6 with black line, but with a reduced P_{TH}.

The design process used for this purpose is similar to the one detailed in [27], where it was explained how to design an interdigital filter with the specifications collected in Table 3. However, in this case where the complexity of the filter has increased due to the insertion of the corrugations, the design process has been completely performed using the commercial software CST Studio Suite [26] and including the corrugations from the beginning, as detailed below.

The first step in the design process consists of characterizing the input/output coaxial excitation. Compared to the previous filter, the new structure under analysis contains the corrugations block, as shown in Fig. 10(a). As the external quality factor, Q_{ext}, must be the same in the two filters, both the height H_1 of the first strip and the position d of the input/output coaxial feedings need to be re-designed. The new obtained dimensions are collected in Table 4, where a slight variation can be observed with respect to the filter with no corrugations.

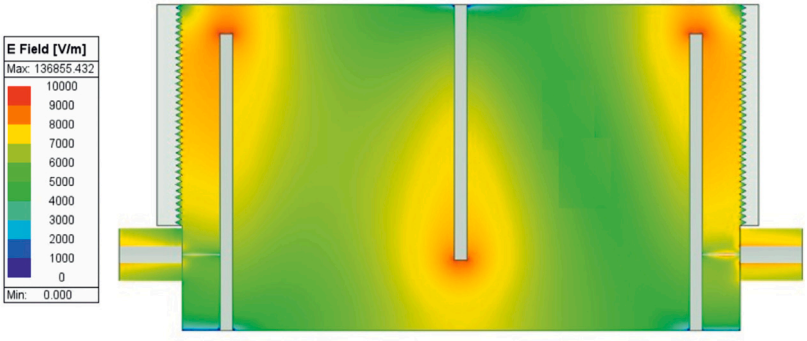

Fig. 7. Electric field intensity distribution (f_c = 3 GHz) -longitudinal section view- after inserting the corrugations in the interdigital 3rd-order band-pass filter.

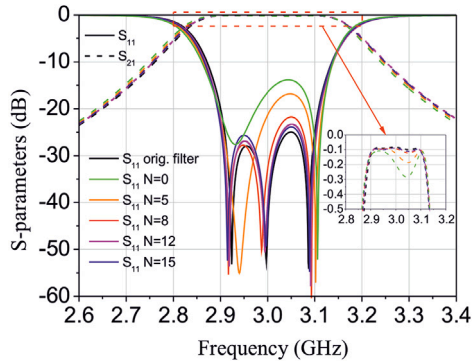

Fig. 8. Comparison of the electrical response of the original interdigital band-pass filter (without corrugations) with the corrugated filter when removing a different number N of corrugations.

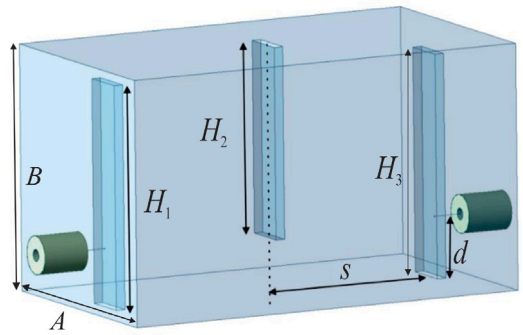

Fig. 9. 3D model of the original interdigital filter with its main dimensions (with $A = B = 26$ mm).

Table 3
Interdigital filter specifications.

Filter type	Band-pass (Chebyshev)
Center frequency	3 GHz
Order	3
Bandwidth	200 MHz
Fractional bandwidth	6.67%
Return losses	25 dB
Waveguide dimensions	$A \times B = 26$ mm $\times$ 26 mm

In the next step, the coupling between resonators is addressed. As it is well known, the EM coupling between resonators depends on the distance s between the flat strips. The topology depicted in Fig. 10(b) is used to obtain an initial value for the distance s, taking into account the required value for the coupling coefficient. Since the corrugations hardly modify the electrical response of the component, the new value obtained for the spacing between the strips is very similar to the one we obtained for the filter without corrugations, as we can observe in Table 4.

Table 4
Dimensions of the designed interdigital filters: without corrugations vs. with corrugations (designed and optimized)

	Without corr. [mm]	With corr. (designed) [mm]	With corr. (optimized) [mm]
$H_1(=H_3)$	23.683	23.550	23.590
H_2	20.320	20.280	20.323
s	17.721	17.500	17.929
d	6.076	6.080	6.924

Table 4 collects the dimensions of the designed interdigital filters, while in Fig. 11(a) a comparison is shown of the electrical response of the original filter (without corrugations, black lines) with that of the redesigned filter with corrugations (red lines). Although the performed redesign procedure has provided a good electrical response in terms of center frequency and return losses, a final optimization step over the obtained redesigned filter dimensions has been done, and whose dimensions are also included in Table 4. In Fig. 11(a), the electrical response of the redesigned filter with corrugations after the final optimization step is also represented (blue lines), where it can be checked that a very good agreement has been achieved in this case with the original filter response. Additionally, for validation purposes, a comparison of the wideband electrical response of this optimized filter, calculated with two well-known electromagnetic simulation tools (Ansys HFSS and CST), can be seen in Fig. 11(b), showing a very wide rejection band (up to 7.7 GHz), and revealing a very good agreement between both computed electrical responses in all the analyzed frequency range, thus validating the obtained response.

We have also represented the group delay of the filter within the passband (see Fig. 12(a)), showing little variation with frequency (from 0.5 to 3 ns). We have also calculated the unloaded Q factor for the two different resonators considered in the designed filter. In this regard, note that, in contrast to the central resonator, the input/output resonators include a corrugated surface in the front/back wall of the rectangular enclosure. To do that, the eigenmode solver of the commercial software Ansys HFSS has been employed, using an equivalent conductivity value of $3.8 \cdot 10^7$ S/m (aluminium). The obtained values are $Q_u = 1542$ for the central resonator, and $Q_u = 1394$ for the input/output resonators including the corrugated surface. On the other hand, if the formula (4.147) collected in [29] is used to compute the filter quality factor, a value of 1506 can be obtained.

On the other hand, we have conducted a sensitivity analysis regarding manufacturing tolerances in the final filter (with corrugations), considering 17 design parameters (regarding the different filter geometrical dimensions), to which we have applied a 10-μm tolerance using a uniform distribution criterion. This study has been carried out using the

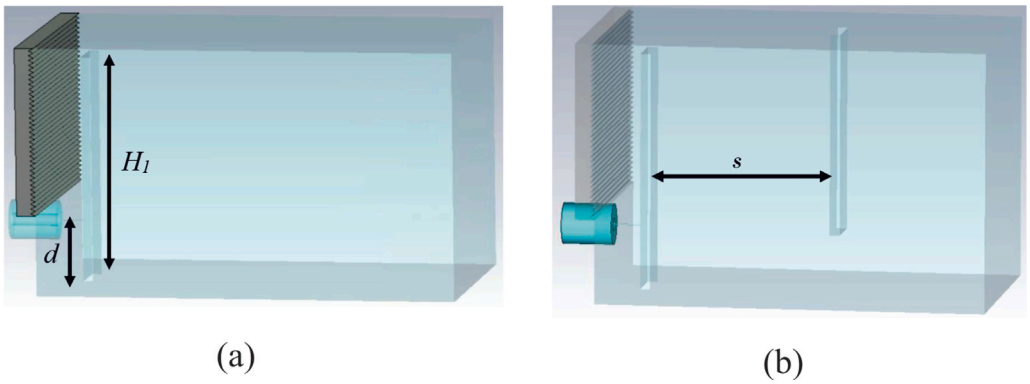

Fig. 10. (a) Structure used for determining the values of $H_1(= H_3)$ and d of the redesigned interdigital filter, and (b) of the distance s between resonators.

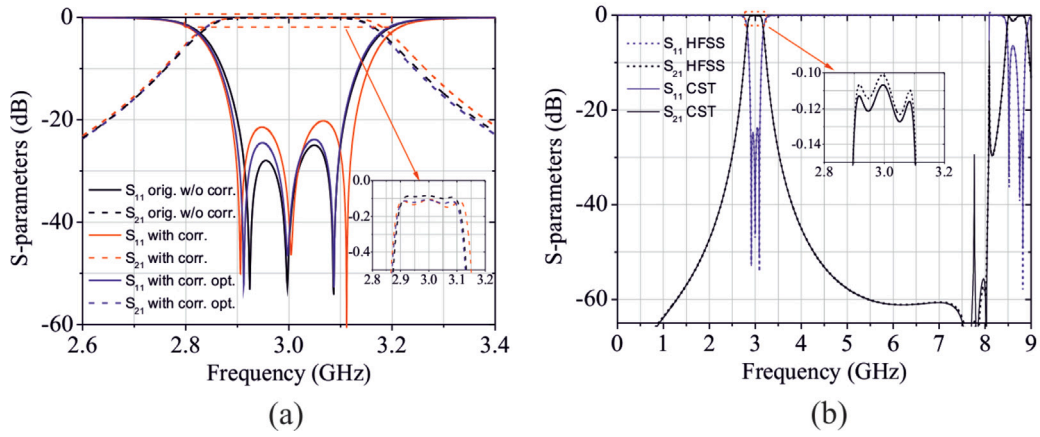

Fig. 11. (a) Comparison of the electrical response of the original filter (without corrugations, black lines) with that of the redesigned filter with corrugations, with red lines, and after the final optimization step, with blue lines. (b) Comparison of the wideband electrical response of the final optimized filter with corrugations calculated with two well-known electromagnetic simulation tools (Ansys HFSS and CST.). (For interpretation of the references to color in this figure legend, the reader is referred to the web version of this article.)

"Statistical" tool in HFSS, and the results obtained for 100 iterations have been included in Fig. 12(b). Additionally, a sensitivity analysis has also been done regarding the corrugations dimensions, to analyze the effect of possible variations of the corrugations depth, considering 20-μm steps around the design value (t = 500 μm) and the results have been included in Fig. 12(c). These good results allow to conclude the potential manufacturing of the designed filter, without the need of using additional tuning screws, using a high-precision (with 10-μm tolerances) milling technique available in the market.

Additionally, the computed P_{TH} of the final optimized filter with corrugations is 425 W, which is still a 150% higher than that of the original filter, thus fully validating the proposed approach. Finally, Table 5 shows a comparison between the results of this work and other studies in the literature regarding the reduction of multipactor effect, which stands out the proposed approach in this work in terms of multipactor reduction, with demonstrated lifetime and reproducibility (differently from those using material coatings or micro-porous surfaces), and no need of non-standard waveguides, thus avoiding the use of expensive and bulky waveguide transformers.

Table 5
Comparison between the results of this work and other studies in the technical literature regarding the reduction of multipactor effect.

Ref.	Technique	Non-standard waveguides	f_0 (GHz)	Component size (mm)	Increase of P_{TH}(%)
[12]	Micro-porous surfaces	No	11.8	40.0 × 20.0 × 110.0	No discharge
[13]	Micro-porous surfaces	No	C-band	–	162
[14]	Material coating	No	0.7	–	No discharge
[17]	Smooth profile	Yes	11.7	19.0 × 9.5 × 218.0	1550
[20]	Dielectric material	No	3.2	72.0 × 5.0 × 80.0	No discharge
[21]	Ridged structure	Yes	1.2	–	150
This work	Corrugations	No	3.0	26 × 26 × 45	150

4. Conclusions

In this work, the impact on the P_{TH} when introducing a surface corrugation profile over different microwave components has been studied, including rectangular and triangular shapes, and with dimensions ranging from tens of microns to millimeters. We have sought to understand how these parameters affect the effectiveness of mitigation of the multipactor effect, and to assess the feasibility of implementing these corrugations in critical areas of an example of filtering structure without degrading its electrical response. This comprehensive approach aims to validate the effectiveness of these techniques in more complex components, and to open up new possibilities for device design and optimization of microwave devices for space applications. Specifically, it has been observed that there is a higher mitigation of the multipactor effect in a waveguide with triangular corrugations compared to rectangular ones. It was also found that the greater the depth of the corrugations, the greater the P_{TH} value, up to a certain limit,

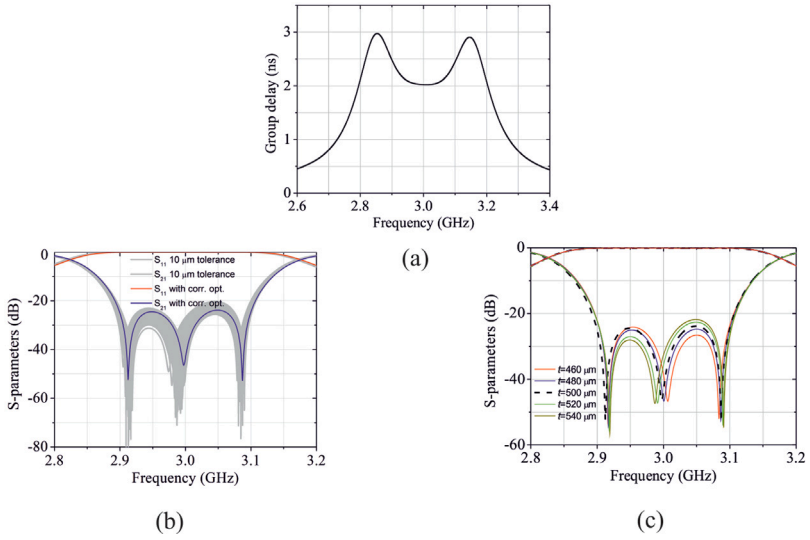

Fig. 12. (a) Group delay of the final optimized filter with corrugations. Sensitivity analysis of the filter with corrugations (b) with 100 iterations and 10 μm of tolerance, and (c) with 5 different corrugation depth values.

which in the case of the RW under study was 0.5 mm. Finally, the triangular profile has been tested with a band-pass filter case with promising results in terms of P_{TH}, even when the electrical response of the filter was affected by the introduction of corrugations, in which case a redesign procedure of the filter dimensions has proved to recover a good electrical response while keeping a great improvement of its power handling capability. The proposed approach in this work stands out with respect to other traditional multipactor reduction techniques, like using material coatings or micro-porous surfaces, and without need of non-standard waveguides, thus avoiding the use of expensive and bulky waveguide transformers, and meeting the highly restrictive requirements (in terms of quality factor or compactness) for filtering components used in space applications. In the near future, it is planned to manufacture the components studied to carry out power tests, in order to obtain experimental validation of the studies performed.

CRediT authorship contribution statement

S.M. Bonte: Writing – original draft, Validation, Investigation, Formal analysis, Conceptualization. **R. García:** Writing – review & editing, Validation, Formal analysis. **A. Coves:** Writing – review & editing, Validation, Supervision, Methodology, Investigation, Funding acquisition, Formal analysis, Conceptualization. **J.M. García-Barceló:** Writing – review & editing, Investigation, Formal analysis. **A.A. San-Blas:** Writing – review & editing, Supervision, Formal analysis. **M. Sancho:** Writing – review & editing, Validation. **M.A. Sánchez-Soriano:** Writing – review & editing, Supervision, Investigation. **V.E. Boria:** Writing – review & editing, Validation, Investigation.

Funding

This work has been funded by the Ministerio de Ciencia, Innovación y Universidades (Spanish Government) through the Subprojects C41 and C43 of the R&D Projects PID2022-136590OB (under grant AEI/10.13039/501100011033/FEDER, UE) and TED2021-129196B (under grant 10.13039/501100011033/Unión Europea NextGenerationEU/PRTR). JMGB thanks the European Research Council grant ERC-2018-StG-802836 (AxScale project), and the Lise Meitner program "In search of a new, light physics" of the Max Planck society.

Declaration of competing interest

The authors declare that they have no known competing financial interests or personal relationships that could have appeared to influence the work reported in this paper.

Data availability

Data will be made available on request.

References

[1] Hatch AJ, Williams HB. Multipacting modes of high-frequency gaseous breakdown. Phys Rev 1958;112:681–5.
[2] Vicente C, Mattes M, Wolk D, Mottet B, Hartnagel HL, Mosig JR, D. R. Multipactor breakdown prediction in rectangular waveguide-based components. In: IEEE MTT-s international microwave symposium digest. Long Beach, CA, USA; 2005, p. 1055–8.
[3] Vague JJ, Asensio I, Coves A, San Blas A, Reglero M, Vidal-Pantaleoni A, Raboso D, Baquero-Escudero M, Boria V. Study of the multipactor effect in groove gap waveguide technology. IEEE Trans Microw Theory Tech 2022;70(5):2566–78.
[4] San-Blas A, Gimeno B, Boria V. Study of the multipactor phenomenon using a full-wave integral equation technique. AEU - Int J Electron Commun 2017;79:286–90.
[5] A. Iqbal PZ. A supervised machine learning framework for multipactor breakdown prediction in high-power radio frequency devices and accelerator components: a case study in planar geometry. 2025, doi: https://www.arxiv.org/abs/2507.17881.
[6] Iqbal A, Wong P, Suresh S, Zhang P, Wen D, Lin S. Multipactor in a coaxial geometry with non-sinusoidal RF fields. In: 2024 joint international vacuum electronics conference and international vacuum electron sources conference (IVEC + IVESC). Monterey, CA, USA; 2024, p. 1–2. http://dx.doi.org/10.1109/IVECIVESC60838.2024.10694963.
[7] Wang G, Aranganadin K, Hsu H, Verboncoeur J, Lin M. A simple space chargel imited emission algorithm for 1-D Particle-in-Cell simulations. In: 2024 joint international vacuum electronics conference and international vacuum electron sources conference (IVEC + IVESC). Monterey, CA, USA; 2024, p. 1–2. http://dx.doi.org/10.1109/IVECIVESC60838.2024.10694976.
[8] Coves A, Torregrosa-Penalva G, Vicente C, Gimeno B, Boria V. Multipactor discharges in parallel-plate dielectric-loaded waveguides including space-charge effects. IEEE Trans Electron Devices 2008;55(9):2505–11.
[9] Sorolla E, Belhaj M, Sombrin J, Puech J. New multipactor dynamics in presence of dielectrics. Phys Plasma 2017;24(10):103508–1–103508–13.
[10] Berenguer A, Coves A, Mesa F, Bronchalo E, Gimeno B. Analysis of multipactor effect in a partially dielectric-loaded rectangular waveguide. IEEE Trans Plasma Sci 2019;47(1):259–65.
[11] Berenguer A, Coves A, Gimeno B, Bronchalo E, Boria V. Experimental study of the multipactor effect in a partially dielectric-loaded rectangular waveguide. IEEE Microw Wirel Compon Lett 2019;29(9):595–7.
[12] Montero I, Aguilera L, Raboso D, Wochner U. Antimultipactor device. 2016, Patent WO2016042192A1, WIPO (PCT), US10724141B2, CA2973088C, ES2564054B1.
[13] Cui W-Z, Li Y, Yang J, Hu T-C, Wang X-B, Wang R, Zhang N, Zhang H-T, He Y-N. An efficient multipaction suppression method in microwave components for space application. Chin Phys B 2016;25:068401.

[14] Ives RL, Oldham C, Gilmore M, Kern IJ. Performance of multipactor coatings applied using atomic layer deposition. In: IEEE international conference on plasma science (ICOPS). Seattle, WA, USA; 2022, p. 1.
[15] Peverini O, Addamo G, Tascone R, Virone G, Cecchini P, Mizzoni R, Calignano F, Ambrosio EP, Manfredi D, Fino P. Enhanced topology of E-plane resonators for high-power satellite applications. IEEE Trans Microw Theory Tech 2015;63(10):3361–73.
[16] Hueso J, Vicente C, Gimeno B, Boria VE, Marini S, Taroncher M. Multipactor effect analysis and design rules for wedge-shaped hollow waveguides. IEEE Trans Electron Devices 2010;57(12):3508–17.
[17] Arregui I, Teberio F, Arnedo I, Lujambio A, Chudzik M, Benito D, Lopetegi T, Jost R, Görtz F-J, Gil J, Vicente C, Gimeno B, Boria VE, Raboso D, Laso MAG. High-power low-pass harmonic filters with higher-order TEn0 and non-TEn0 mode suppression: Design method and multipactor characterization. IEEE Trans Microw Theory Tech 2013;61(12):4376–86.
[18] Lin S, Zhong H, Chen C, Li Y, Cao M, Wong P. Electron migration via transversal electrostatic field for suppressing local-regional multipactor breakdown. In: proceedings of 2024 IEEE international conference on plasma science (ICOPS). Beijing, China; 2024, p. 1. http://dx.doi.org/10.1109/ICOPS58192.2024.10625784.
[19] Huang X, Wang H, Liu L, Liu D, Li Z. Suppression of multipactor discharge on a dielectric with a beat wave. IEEE Trans Electron Devices 2025;72(1):45–452.
[20] Zhai Y, Wang R, Wang H, Cao M, Lin S, Zhang N. Suppressing the multipactor in microwave devices by introducing the dielectric material. IEEE Trans Electron Devices 2025;Early Access. http://dx.doi.org/10.1109/TED.2025.3588521.
[21] Jiang L, Yang F, Cui Z, Yang J. Ridged structure of coaxial cavity for raising the multipactor threshold of microwave switch. IEEE Access 2024;12:105761–5.
[22] Chang C, Li YD, Verboncoeur J, Liu YS, Liu CL. Suppressing double-metal-surface resonant multipactor by three dimensional wavy surface. Phys Plasmas 2017;24:040702.
[23] Coves A, Bonte S, Morales A, Vague JJ, Boria VE, Montero I. Significant reduction of multipactor effect in a rectangular waveguide with periodically grooved metallic surfaces. In: 1st space microwave week 2023. Noordwijk, The Netherlands; 2023, p. 1–4.
[24] Pivi M, King FK, Kirby RE, Raubenheimer TO, Stupakov G, Le Pimpec F. Sharp reduction of the secondary electron emission yield from grooved surfaces. J Appl Phys 2008;104:104904.
[25] ANSYS. High frequency structure simulator (HFSS). 2024, URL https://www.ansys.com.
[26] Dassault Systemes. SPARK3D CST studio suite. 2024, URL https://www.3ds.com/products/simulia/spark3d.
[27] García R, San-Blas AA, Bonte S, Coves A, Sanchez-Soriano MA, Guglielmi M, Boria VE. Design procedure for interdigital waveguide bandpass filters based on flat metallic strips. Radio Sci 2025;60:1–13.
[28] ESA-ESTEC, ESA Publication Division. Multipacting design test. Tech. rep., Noordwijk, The Netherlands: European Cooperation for Space Standarization (ECSS); 2020.
[29] Hunter I. Theory and design of microwave filters. IEE London; 2001.